Microchemistry and microstructure of sustainable mined zeolite-geopolymer

Samar Amari [a], Mariam Darestani [a, b, c, *], Graeme J. Millar [b], Llew Rintoul [a], Bijan Samali [c]

[a] School of Chemistry, Physics and Mechanical Engineering, Queensland University of Technology (QUT), Brisbane, Queensland, Australia
[b] Institute for Future Environments, Science and Engineering Faculty, Queensland University of Technology (QUT), Brisbane, Queensland, Australia
[c] Centre for Infrastructure Engineering, Western Sydney University, Sydney, Australia

ARTICLE INFO

ABSTRACT

Geopolymers are three-dimensional amorphous Si-O-Al networks that generally can be synthesized from low-Ca aluminosilicate mineral sources. Such materials were first introduced as a sustainable construction material but today their application goes beyond the building industry. So far, a broad range of aluminosilicate minerals including fly ash, natural pozzolans, kaolin and metakaolin have been used to produce geopolymers; however, there are limited studies on the geopolymerization of porous and crystalline aluminosilicate minerals such as mined zeolites. Use of zeolite as it is for commercial applications depends on the shape and architecture of these materials. Therefore, the hypothesis was that geopolymerization provides the possibility of using mined zeolite in different shapes. Moreover, zeolite as a nontoxic mineral material with an inherent 3D structure may result in the formation of the cleaner geopolymeric product with different physical properties compared to when waste materials such as fly ash are employed. In this study, the viability of creating geopolymers from mined zeolite has been demonstrated. The aim of this study was to evaluate the influence of different parameters such as zeolite particle size, curing temperature, reagents ratio and time on amorphous content and mechanical strength. The conversion of the crystalline phase of mined zeolite to amorphous gel and/or synthetic zeolite phases was comprehensively studied using X-ray diffraction. It was found that finer zeolite particles resulted in the formation of a material with higher amorphous content (max ~60%) and higher mechanical strength (max ~33 MPa). It was also shown that the higher amorphous content did not necessarily translate to higher mechanical strength due to the formation of intermediate species that cannot transfer into the polycondensation stage. It was revealed that the formation of analcime and chabazite may occur through the geopolymerization process. Microstructure studies using infrared spectroscopy confirmed the geopolymer formation and development over time.

© 2019 Published by Elsevier Ltd.

1. Introduction

Geopolymers are three-dimensional amorphous Si-O-Al networks that generally can be synthesized from low-Ca aluminosilicate mineral sources using a strong alkaline activator (Hajimohammadi and van Deventer, 2016; Provis and Bernal, 2014). It is believed that the use of geopolymers goes back to the ancient Egyptians, but geopolymerization as we know it today, was first defined by Davidovits in 1978 (Rao and Liu, 2015). These materials are considered an environmentally friendly alternative to cement in the construction industry (Reddy et al., 2016). This is because the geopolymer production releases about six times less CO_2 in comparison to production of Portland cement. These materials have great potential for various applications due to their sustainable inherent features such as being lightweight, fire resistant, of high workability and good chemical stability (Aguirre-Guerrero et al., 2017; Cheng and Chiu, 2003; Majidi, 2009). Some of the applications are production of light weight construction material (Pimraksa et al., 2011), heavy metal stabilization (El-Eswed et al., 2015), manufacturing high quality, non-burning and fire resistant ceramic breaks (Liew et al., 2016a), and thermal insulation (Ferone et al., 2019).

Geopolymerization is a low-cost method to convert different

---

types of inorganic supplies from waste materials to natural resources into a more valuable, environmentally friendly product.

So far a broad range of aluminosilicate minerals including fly ash(Mehta and Siddique, 2016), natural pozzolans (Ghafoori et al., 2016), kaolin and metakaolin (Xu and van Deventer, 2003) have been used to produce geopolymers. The use of kaolin for geopolymer formation produced a relatively weak structure due to its low surface area; which minimized the dissolution rate of Si and Al by alkali reactant and limited gel formation (Ming, 2011). The calcined form of kaolin (metakaolin) with higher amorphous phase content has therefore been preferred for geopolymerization; albeit, it may still be too soft for construction use (Liew et al., 2016b). Fly ash has been extensively employed as source material for geopolymerization processes as it is considered a cost-effective alternative to conventional binder materials (Wang et al., 2007). Besides Al, Si, Ca and Fe, fly ash contains several toxic trace metal components such as Hg, Pb, and Cr with levels even higher than those of coal (Nyale et al., 2014). Consequently, the hazardous nature of this material restricts its commercial application. Natural pozzolans are amorphous or glassy aluminosilicate materials (Najimi, 2016). Bondar *et al.* (Bondar et al. (2007) activated Iranian natural pozzolans, using several blends of sodium silicate and KOH to make a geopolymer with a maximum mechanical strength of 18 MPa. However, long setting times were required which reduced the attractiveness of using this material (Najimi, 2016).

Surprisingly, there are limited reports describing geopolymerization of porous aluminosilicate minerals, such as mined zeolite. Mined zeolites are abundant, relatively inexpensive, physically stable, of well-defined structure, and display cation exchange capacity (Castaldi et al., 2005). Regarding the unique properties of zeolite, zeolite-based geopolymer may be appropriate for a greater range of applications than simply construction materials which have been the primary focus until now. For instance, Ortega et al. (2000) activated clinoptilolite using $Ca(OH)_2$ and reported that the mechanical properties of the resulting product depended upon the: curing time; temperature; the quantity of $Ca(OH)_2$; and zeolite particle size. The maximum compressive strength of the binders was reported to be 38.7 MPa (Ortega et al., 2000). Similarly, Villa et al. (2010) studied the synthesis conditions for Mexican zeolite-based geopolymers for construction applications. They concluded that increasing curing time (up to 90 days) resulted in a higher mechanical strength for the geopolymer regardless of temperature or activator ratios (Villa et al., 2010). Nikolov et al. (2017) evaluated the effect of three different types of activator solutions *i.e.* sodium silicate, sodium hydroxide and sodium carbonate with different concentrations on geopolymerization of Bulgarian zeolite. These authors concluded that the highest compressive strength of 3.7 MPa was attained after four weeks when sodium silicate was solely used as an activator (Nikolov et al., 2017). Composite geopolymers which comprised of both mined zeolite and kaolin clay have also been reported for applications such as stabilization of heavy metals (El-Eswed et al., 2015) and for CO_2 adsorption (Papa et al., 2018).

Use of zeolites for commercial applications depends on the shape and architecture of these materials. For example, water treatment using zeolite is achieved by passage of water through columns containing relatively large particles (0.5–2 mm). However, not only is rapid breakthrough observed due to diffusion problems but also the regeneration of such zeolite columns is a time-consuming process (Dehghan and Anbia, 2017). Therefore, geopolymerization of zeolites could provide an alternative mean of transforming these materials into innovative shapes which promote performance. In addition, fine grades of zeolite, which are not suitable for water columns due to pressure drop limitations, can potentially be employed by geopolymerization.

From literature evaluation, the use of mined zeolites to make geopolymer materials appears to have several gaps in knowledge. For example, the geopolymerization reaction mechanism, and the chemical and thermal stability of the final product are not well defined. Therefore, the objective of this study was to investigate the feasibility of geopolymerization of mined zeolite. The hypothesis was that mined zeolites may form unique geopolymer materials due to the inherent 3D nature of the starting material. Specific research questions to address include: (1) what is the effect of particle size on the polymerization rate and mechanical strength of final products? (2) Can the properties of zeolite-based geopolymer be manipulated by changing reaction time and temperature? (3) Does the concentration of the alkaline reagent, the ratio of activator, and solid to liquid ratio have any effect on geopolymer properties? (4) Are any other crystalline phases formed in the geopolymerization process? Consequently, we examined the effect of various geopolymer synthesis parameters at laboratory scale using mined zeolite sourced in Australia. Various techniques were used to characterize the geopolymer including X-ray diffraction, X-ray Fluorescence, electron microscopy, vibrational spectroscopy, and thermal analysis.

2. Materials and methods

2.1. Zeolite

Mined zeolite was supplied from a mined in Australia in a range of mesh sizes. Zeolite samples were dried at 60 °C for 24 h in an oven before use.

2.2. Chemicals

Sodium hydroxide pellets were purchased from Chem-Supply Pty Ltd and were dissolved in water to prepare the alkaline reagent for polymerization. Liquid sodium silicate (45% concentration) with a molar ratio of $SiO_2/Na_2O = 2:3.3$ was purchased from Redox Pty Ltd and used without any further purification or pretreatment.

2.3. Geopolymer preparation

Sodium hydroxide (10M, pH: 12.8) as the main reagent and liquid sodium silicate (pH: 12.3) as the activator were used for geopolymerization of mined zeolite. A mechanical mixer at a speed of 300 rpm was used to mix the raw mineral with reagents for 10 min. Geopolymer samples were prepared using different zeolite average particle sizes ranging from 54 μm to 1 mm and then the resulting slurry was cast into cylindrical moulds of 10 mm high and 5 mm diameter for use in mechanical tests. Samples were cured for 1–4 weeks in an oven at specified temperatures. After finding the desirable particle size, in terms of mechanical strength, the effect of different experimental parameters on the properties of geopolymers was studied using the best zeolite particle size (*i.e.* 54 μm). For this, samples were cast into larger standard cylindrical moulds of 100 mm high and 50 mm diameter and were cured for 1–4 weeks in an oven at specified temperatures. After curing, samples were removed from the polypropylene moulds and stored in airtight zipper bags for characterization. A schematic description of the mined zeolite geopolymer production is shown in Fig. 1. The effect of sodium hydroxide concentrations (8, 10, and 12 M) with a pH value of 12.6, 12.8 and 13.1 respectively, and the sodium silicate/sodium hydroxide mass ratio (1, 2, and 4) was also examined. The impact of solid content was also studied by preparing samples with total solid/liquid mass ratios of 0.75, 1, and 1.3. All samples and their corresponding characterization were made in triplicate and data
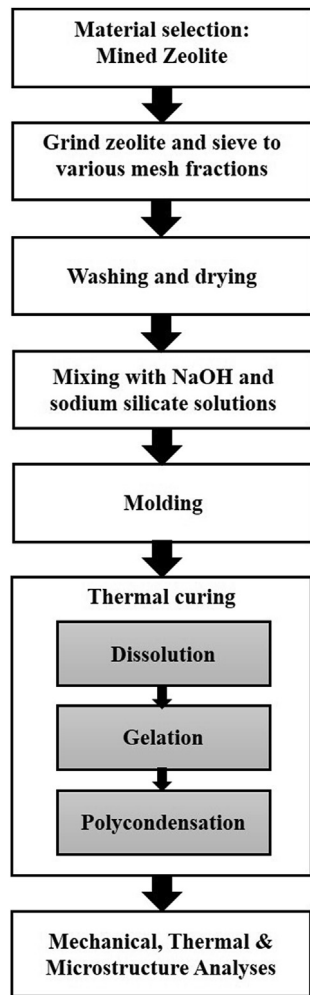
Fig. 1. Schematic description of the mined zeolite geopolymer production.

then averaged. Sample codes and details of polymerization conditions for each sample prepared are summarised in Table 1.

2.4. Characterization techniques

2.4.1. Material compressive strength

The compressive strength of geopolymer samples was tested according to ASTM C 39/C 39M−03 using the Instron universal testing system (USA). The pressure was applied at a rate of 0.1 mm/min and the pre-load force was 50 N.

2.4.2. Particle size distribution

Particle size distribution was analysed using a Mastersizer 3000 instrument (Malvern PAN analatical, Netherlands) with a stirrer speed of ~3000 rpm. The samples were continiously added to dionized water until the obscuration reached an acceptable level of 10%. The samples were dispersed for 20 s prior to performing the measurment.

2.4.3. Scanning Electron Microscopy (SEM)/Energy Dispersive Spectroscopy (EDS)

Scanning Electron Microscopy (SEM) coupled with chemical analysis by Energy Dispersive Spectroscopy (EDS), (JEOL 7001f, Japan) was used to determine the morphology and surface composition of samples before and after polymerization. Prior to use, the samples were mounted on sample holders using conductive adhesive carbon tabs and were gold (99.99%) coated using a Leica EM SCD005 − cool sputter coater, under argon. The pressure of the gold sputter vacuum chamber was 0.05 mbar and the sputter current was 30 mA. Then the specimens were viewed under the SEM with an accelerating voltage of 10 kV and secondary electron images taken at various magnifications.

2.4.4. X-ray diffraction (XRD)

X-ray diffraction (XRD) using an X'Pert Pro diffractometer working at 40 kV and 40 mA with a cobalt source (PANalytical, Netherlands) was used to characterize the crystalline phases in the zeolite and geopolymer samples. Samples were prepared for X-ray powder diffraction using a corundum (Al_2O_3, Baikowski International) internal standard with a specific wt % to an accurately weighed portion of the geopolymer samples. Then, 10 mL ethanol was added to specimens (including corundum) and micronized using a McCrone mill and zirconia beads for 6 min. Then the slurries were set in an oven at 40 °C for 12 h. The resultant uniform powders were back-loaded and pressed into sample holder disks. The samples were rotated during analysis. The incident optics were a 15 mm mask, 0.04 radian Soller slits, a 0.5° fixed divergence slit and a 2° fixed anti-scatter slit. The diffracted beam optics before the X'Celerator detector were an iron Kβ filter, a 5 mm fixed anti-scatter slit, and 0.04 radian Soller slits. Patterns were gathered at a step size of 0.016° from 5 to 90 °2θ. The total measurement time was 30 min per sample. Phase identification was achieved by PANalytical Highscore Plus (V4) and MDI Jade (V4.1) with various databases (PDF4+, American Mineralogist Crystal Structure Database 2010; Crystallographic Open Database, and ICSD FIZ Karlsruhe). Quantitative phase analysis was carried out using the Rietveld method as implemented in TOPAS (V5, Bruker).

2.4.5. X-ray fluorescence (XRF)

X-ray Fluorescence (XRF) was employed to identify the major elements of the zeolite and geopolymer samples. For sample preparation 1.15 g of material was mixed with 8.85 g of a 50:50 mix of lithium metaborate ($LiBO_2$) - lithium tetraborate ($Li_2B_4O_7$) flux containing 0.5 wt% lithium iodide (LiI) as a wetting agent; and then melted for 25 min at 1050 °C. A Claisse TheOx automated fusion

Table 1
Sample codes and variables examined in preparing geopolymer samples.

Sample Name	Zeolite/liquid ratio	Sodium silicate/Sodium hydroxide ratio	Temperature (°C)	NaOH concentration (M)
GPS1	1.3	1	60	10
GPS2	1.3	2	60	10
GPS3	1.3	4	60	10
GPS4	0.75	2	60	10
GPS5	1	2	90	12
GPS6	1	2	60	12
GPS7	1	2	60	8
GPS8	1	2	60	10

device was used for sample glass discs preparation. Elements were identified on 40 mm diameter glass discs. A PANAlytical Axios wavelength dispersive (WD) X-ray Fluorescence spectrometer armed with a 1 kW Rh tube was utilized. The device also equipped with PX1, PE002, LiF200 and LiF220 analysing crystals, scintillation, duplex, and P10 flow proportional counters, tube filters, and 700 μm and 300 μm collimators. Element percentages were obtained using PANAlytical's WROXI application. Loss-On-Ignition (LOI) resulted from another analysis procedure. Major element data are reported as oxide%.

2.4.6. Fourier transform infrared spectroscopy (FT-IR)

Fourier-transform infrared spectroscopy (FT-IR) was performed using a Nicolet iS50 instrument equipped with a single bounce diamond ATR (Thermo Scientific, Madison, USA). Spectra were recorded by accumulating 64 scans at 4 cm^{-1} resolution.

2.4.7. Thermogravimetric/differential scanning calorimetry (TG/DSC)

Differential scanning calorimetry (DSC) and thermogravimetric (TG) analysis were performed using an STA 449F3 TG-DSC instrument (Netzsch, Germany) under nitrogen atomosphere with the heating rate of 100°C/min to characterize thermal behaviour of the raw material and geopolymers.

Table 2 summarizes the characterization techniques, model and methods were employed.

3. Results and discussion

The characterization of the mined zeolite used is presented in the supplementary section for reference. In summary it comprised of SiO_2 (67.49%), Al_2O_3 (12.18%), CaO(3.04%), K_2O(1.83%) and Fe_2O_3(1.43%), trace amount of MgO, Na_2O, TiO_2 and P_2O_5 with Loss On Ignition (LOI) of 11.9% using XRF analyses which was in agreement with previous studies (Millar et al., 2016). The Si/Al molar ratio of mined zeolite was acquired 4.9.

X-ray diffraction revealed that zeolite mainly consisted of clinoptilolite/heulandite (28.1%), quartz (~20%), stilbite (19.1%), minor quantities of feldspar, mordenite, plagioclase and chabazite. 21.4% of the zeolite was unidentified including the amorphous content which was possibly due to the presence of non-crystalline components such as amorphous glass (Elaiopoulos et al., 2010) and the trace amount of smectite.

Particle size distribution of two zeolite samples of fine particle size grade (nominally 0 to 0.125 and 0.125–0.5 mm) were characterized. Particle size analysis showed that these zeolite samples had particles both ranged from 0.2 to 200 μm in size and exhibited two

peaks; one around 0.7 μm and another about 45 μm. Interestingly, the sample with a larger average particle size also had a peak around 0.7 μm that could be due to the presence of smectite which was observed in XRD patterns.

3.1. Effect of zeolite particle size on geopolymerization

To investigate the effect of particle size on geopolymerization progress, four different zeolite particle sizes of A: (0–0.125 mm), B: (0.125–0.5 mm), C: (0.5–0.85 mm) and D: (0.85–1 mm) were chosen. Geopolymer samples with a solid/liquid mass ratio of 1.3, and sodium silicate/sodium hydroxide mass ratio of 1; were prepared and cast into cylindrical moulds of 10 mm high and 5 mm diameter, then synthesized at 60 °C for a period of 1–4 weeks. Quantitative XRD analysis [Table 3] revealed that the percentage of crystalline phases present was significantly impacted by zeolite particle size. The original XRD patterns collected are shown in supplementary section for reference.

Primary trends observed were the decrease of clinoptilolite/heulandite, stilbite and the mordenite with curing time; and the substantial formation of a new amorphous phase. More in depth analysis of the impact of curing time and zeolite particle size upon formation of the amorphous phase is shown in Fig. 2a.

The data are shown in Fig. 2a indicated that the major developments of amorphous content (presumably geopolymer) in all samples occurred within approximately 1 week of contact. This result was in agreement with the study of Panda et al. (2017) who made geopolymers using fly ash and noted a reduction in XRD crystalline peak intensity and corresponding growth of amorphous content due to the dissolution of fly ash in the alkaline solution. It was apparent that the smaller the zeolite size fraction used, the greater the amount of amorphous phase created. Geopolymerization involves three steps: (1) dissolution of the aluminosilicate material; (2) gelation; and (3) polycondensation. It was surmised that the smaller zeolite particles could dissolve at a faster rate than the larger grains (Xu and Van Deventer, 2000). This idea was in accord with a previous study which showed that the reaction kinetics of geopolymer formation increased as the metakaolin particle size decreased (Rahier et al., 2003). Mass transport considerations indicated that metakaolin particle size and/or its surface area, significantly impacted the rate and degree of dissolution during geopolymerization (Rahier et al., 2003). It has also been postulated that the homogeneity of the formed gel was dependent on the particle size and uniformity of the starting aluminosilicate material (Fernandez-Jimenez et al., 2005). Notably, after 2 weeks of curing, there was a general slight decrease in amorphous content for all zeolite samples studied. This observation may indicate that a

Table 2
Characterization methods.

Analytical techniques	Model	Method
Material Compressive Strength	Instron universal testing system	0.1 mm/min with the pre-load force 50 N
Particle Size Distribution	Malvern Master-sizer 3000	–
Scanning Electron Microscopy (SEM)/Energy Dispersive Spectroscopy (EDS)	JEOL 7001f	Secondary Electron Images with accelerated Voltage of 10Kv on gold (99.99%) coated samples
Gold coater	Leica EM SCD005	Vacuum pressure: 0.05 mbar, Sputter current: 30 mA
X-Ray Diffraction (XRD)	PANalytical	X'Pert Pro diffractometer working Voltage: 40 kV and Current: 40 mA with cobalt source. Internal standards: Corundum
X-ray Fluorescence (XRF)	PANAlytical Axios wavelength dispersive (WD) XRF	40 mm diameter glass discs
Fourier Transform Infrared Spectroscopy (FT-IR)	Nicolet iS50 instrument	Accumulating 64 scans at 4 cm-1 resolution
Thermogravimetric/Differential Scanning Calorimetry (TG/DSC)	STA 449F3 -TG-DSC instrument	Nitrogen atmosphere, Heating rate 10 °C/min

Table 3
Quantitative XRD phase analysis for geopolymers synthesized from mined zeolite with particle sizes of 0−0.125 mm and 0.125−0.5 mm.

Phase	Mined zeolite (%)	Sample A (0−0.125 mm)				Sample B (0.125−0.5 mm)			
		Week1	Week2	Week3	Week4	Week1	Week2	Week3	Week4
Quartz	20	15.5	16.3	15.7	15.1	17.1	13.9	15.5	16.3
Plagioclase (Andesine, Albite)	3.5	3.1	2.8	2.5	2.7	4.2	3.6	4	3.7
K-Feldspar (Orthoclase, Sanidine)	5.5	3.5	4.1	3.2	3.5	3.6	2.8	3.4	3.7
Chabazite	0.2	0.4	0.5	0.5	0.5	0.4	0.4	0.3	0.5
Clinoptilolite/Heulandite	28.1	11.4	8.1	10.9	11.5	14.6	12.8	13.7	14.4
Mordenite	2.2	1.4	0.7	1.6	1.5	1.5	1.3	1.3	1.4
Stilbite-Na	19.1	10	9.3	10.6	10.1	9.5	8	8.7	8.6
Unidentified/Amorphous	21.4	54.7	58.2	55	55.1	49.1	57.2	53.1	51.4
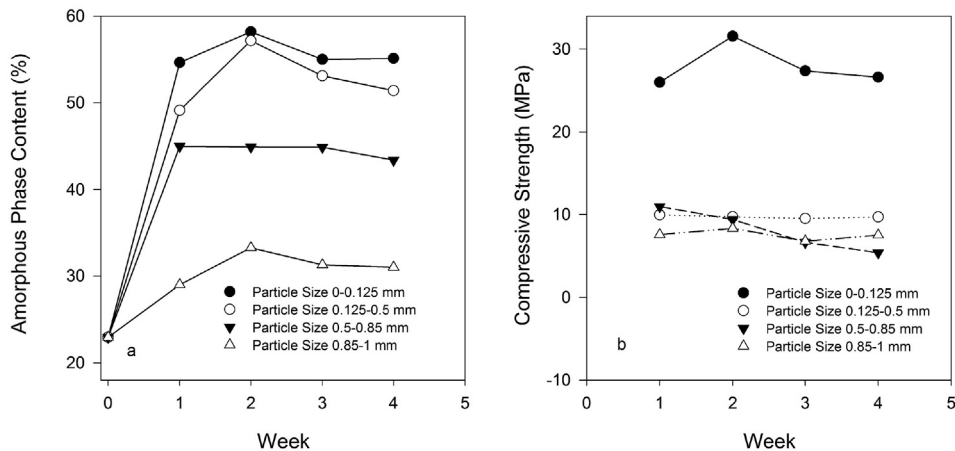
Fig. 2. (a) Amorphous phase content and (b) compressive strength (MPa) of geopolymers prepared using zeolite size fractions as indicated at a temperature of 60 °C.

lack of NaOH within the geopolymer matrix may occur which allows the dissolved Si and Al species to re-join and form a crystalline structure. The fact that Table 3 indicated a slight increase in clinoptilolite/heulandite crystallinity after 2 weeks reaction supported this hypothesis. Note, heulandites and clinoptilolite have similar structural topology, but their natural formation conditions are different (Mumpton, 1960).

Fig. 2b revealed that the compressive strength of the sample made with the smallest particle size reached 33 MPa after 2 weeks and then slightly decreased. Furthermore, the remaining three zeolite size fractions all made geopolymers with similar mechanical strength. The extent of the amorphous phase content is known as an important factor which influences the mechanical and physical properties of geopolymers. A greater amount of the amorphous phase may provide a geopolymer with better mechanical properties (Panda et al., 2017). It has been reported that the fineness is a crucial factor in determining physical properties of fly ash based geopolymers with <43 μm particles giving the highest compressive strength (Komljenovic et al., 2010). Mechanical activation of fly ash which resulted in the particle size reduction also resulted in strength enhancement (Temuujin and van Riessen, 2009).

However, this investigation has shown that increasing amorphous content in zeolite-based geopolymers does not directly promote mechanical strength. In Fig. 2a the 0.125−0.5 mm particles had almost the same degree of amorphous content as the finest zeolite particles but the mechanical strength was not improved compared to that of the largest zeolite grains.

Based on previous literature (Xu and Van Deventer, 2000), both the dissolution step and the gelation formation depend on the mineral particle size. Equation (1) (Xu and Van Deventer, 2000) shows the general process of the geopolymerization reaction.

$$Al - Si \ minerals \ (s) + MOH \ (aq)$$
$$+ Na_2SiO_3(aq \ or \ s) \rightarrow \left[M_z(AlO_2)_x(SiO_2)_y \cdot nMOH \cdot mH_2O \right] gel \tag{1}$$
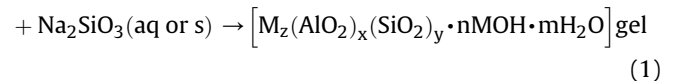
where M is alkali metal. Geopolymerization occurs at the interface of zeolite particles and NaOH, and a gel layer in turn forms on the zeolite surface. This gel can then expand into the gaps between zeolite grains to reach another particle (van Jaarsveld et al., 2003). Finer particles have a higher specific surface area which eventually leads to greater reaction conversion (Mehta and Siddique, 2016). Moreover, the dissolution rate of Si and Al species is highest for the finer particle sizes due to the higher surface area (Mehta and Siddique, 2016). It is also understood that using an ultra-fine grade of materials, can decrease the initial porosity of the mixture which can lead to a denser microstructure, higher workability and strength (Mehta and Siddique, 2016).

When mid-range zeolite particle sizes were used the effect of particle size on amorphous content was more significant than its effect on mechanical strength of the geopolymers. One explanation was that for the sample with mid-range particle size, although dissolution happened, and the gel layer formed; the bonding between neighbouring zeolite grains was limited due to the low surface area and low availability of Si and Al to be dissolved. In addition, the distance between particles was increased which again limited diffusion of the formed gel layer.

Fig. 3 shows a schematic of the effect of the particle size on the geopolymerization process and the theory developed in this study. The results of XRD and compression tests showed enhanced diffusion of alkaline reagents (due to higher surface area of small particles) resulted in higher rates of dissolution and gelation.

Higher gelation rate improved binding among small particles which resulted in greater mechanical strength. In larger particle sizes, the gelation was not enough to completely bind the particles and occupy free volume in the final product. Therefore, in spite of the high amorphous content, the mechanical strength was relatively low. With large zeolite particles (0.85—1 mm) the low surface area limited the diffusion rate of alkaline reagent and resulted in low gelation. Therefore, the amorphous phase was not high and the bond between particles was weak; hence, mechanical strength was low.

3.2. Importance of sodium silicate/sodium hydroxide ratio

Ultra-fine grade zeolite with an average particle size of 54 μm was used for the rest of the experiments. Three samples with different sodium silicate/NaOH mass ratios of 1, 2, and 4 were synthesized. The sample codes (GPS1, GPS2, and GPS3) and the experimental conditions are given in Table 1. General observations from quantitative XRD revealed that the content of chabazite during geopolymer development increased significantly (up to *ca.* 8%) for the sample with the lowest sodium silicate/NaOH ratio. In addition, the amount of quartz percent steadily reduced with time as did the quantity of clinoptilolite/heulandite. The percentage of stilbite and feldspar decreased until 2 weeks of geopolymerization and then slightly increased. Overall, plagioclase and mordenite diminished in percent after 4 weeks of reaction. To gain a better understanding of the results and find a relationship between reaction time and the operational parameters, the amorphous phase value (data from XRD) of each sample is plotted against time [Fig. 4].

As can be seen in Fig. 4a there was a sharp increase in the amorphous phase content in all samples during the first seven days; which indicated the dissolution of zeolite and start of geopolymer synthesis. A sodium silicate/sodium hydroxide ratio of 1 resulted in over 40% amorphous structure in the first week and reached almost 60% in two weeks, then remained almost constant during the next two weeks. By doubling the sodium silicate/sodium hydroxide ratio (GPS2), the amorphous content increased rapidly to
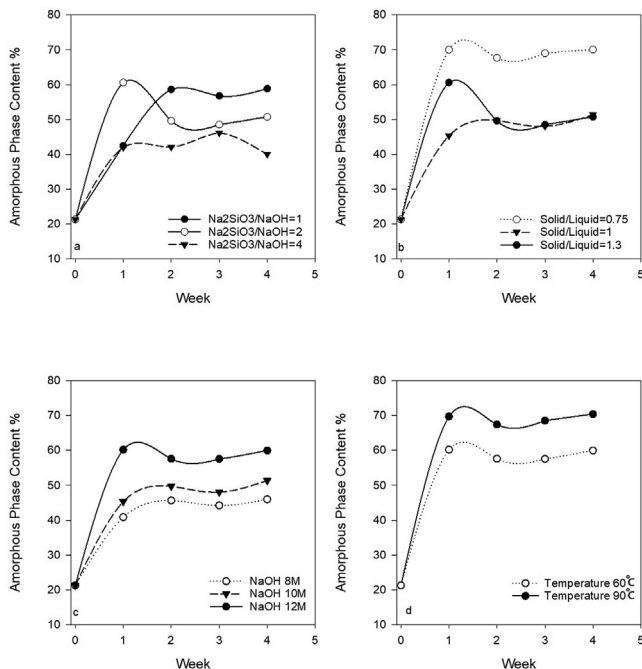

Fig. 4. Amorphous phase changes of geopolymer samples with different (a) Sodium silicate/NaOH ratio, (b) zeolite/liquid Ratio, (c) NaOH concentration and (d) Temperature over 4 weeks.

60% during the first week, but then declined to 50% during the second week; and did not change significantly afterwards. This relatively high amount of amorphous phase after seven days of curing in sample GPS2 was possibly due to the enhanced dissolution of Si and Al species (Hajimohammadi et al., 2011). Although, it is believed that alkali hydroxide is the main reason for the dissolution process, it has been shown that increasing the sodium silicate content can also affect the dissolution rate (Liew et al., 2012). It seems the additional silicate accelerated the dissolution of Al from
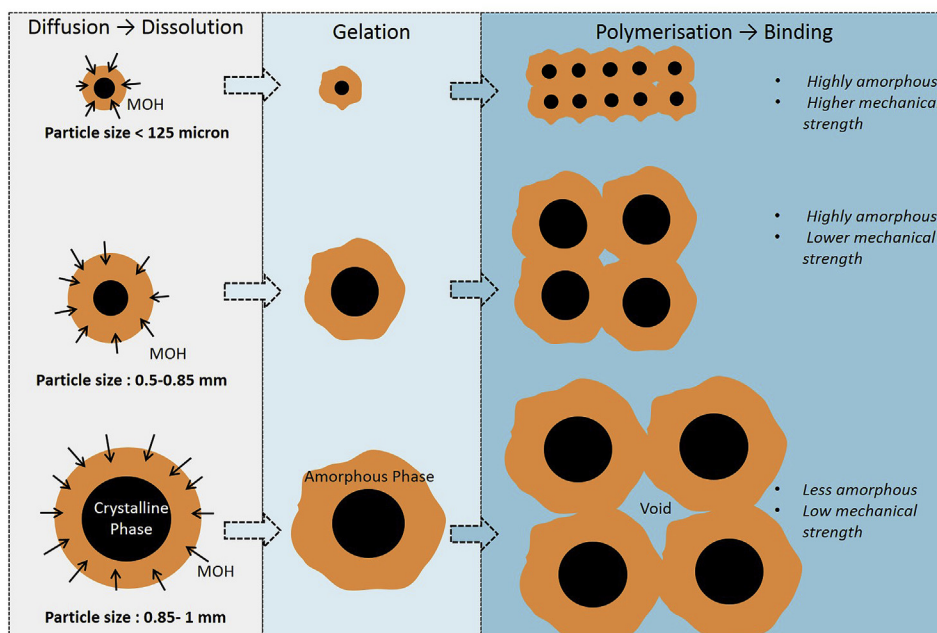

Fig. 3. Schematic of the effect of zeolite particle size on the geopolymerization.

zeolite particles and broke down the structure. Then with sufficient free Al and Si species available, the gelation started; followed by the polycondensation and formation of a three-dimensional amorphous aluminosilicate network, *i.e.* geopolymer.

The decline in the amorphous phase at higher sodium silicate ratios can be explained by investigating XRD patterns of sample GPS2 after four weeks of curing [Fig. 4]. Comparing XRD patterns of GPS2-Week1 (after one week of curing) and GPS2-Week2 (after two weeks of curing) indicated that the crystalline phase increased and resulted in a lower amorphous content after two weeks. This result was in agreement with previous work on geopolymers (Hajimohammadi et al., 2011), and suggested that for samples with higher silicate content, the extra Al and Si species may re-join and form new silica-rich crystals. This phenomenon was not observed for sample GPS1 after one week possibly because of the low amount of sodium silicate that not only does not favour Si-rich crystal formation but also exhibits a slow dissolution rate of the zeolite. A slight decline in amorphous content of GPS1 suggested that after two weeks when sufficient Si and Al were released from aluminosilicate; crystal formation occurred in the sample with sodium silicate/sodium hydroxide of one.

Formation of new silica-rich crystals in the presence of high sodium silicate concentration can also explain the low amorphous content obtained when using high sodium silicate/sodium hydroxide ratio of 4, *i.e.* GPS3. The amorphous phase content of sample GPS3 increased after seven days of curing, then after some small fluctuations in value, reached to approximately 40%. This value was significantly lower than the amount achieved using sodium silicate/sodium hydroxide ratios of 1 and 2. These results suggested that the dissolution rate in sample GPS3 with the highest silicate content was higher than the other samples. One possible explanation was that the dissolution and crystallisation occurred at the same time due to the excessive amount of silicate in sample GPS3.

The amorphous phase content can be indicative of both the geopolymerization progress and the destruction of aluminosilicate crystals. A good example is sample GPS2 that exhibited high amorphous phase content after one week which then declined dramatically along with the formation of crystals during the second week. This behaviour indicated that a significant part of the amorphous phase could be attributed to the free Si and Al species resulting from the destruction of zeolite crystals.

More information was extracted regarding the geopolymerization process by the collection of FTIR spectra of the materials. The general spectra of geopolymer samples are shown at supplementary section. Also illustrated was the FTIR spectrum of mined zeolite to facilitate comparison. Closer inspection of the peak position shifts relating to T-O-Si and water revealed important changes during the geopolymerization process [Fig. 5]. In all samples, the T-O-Si peak position shifted to lower wavenumbers after seven days and later moved to higher wavenumbers. Shifts to lower wavenumbers are reported to be due to the creation of Al-O-Si bonds over the formation of Si-O-Si (Provis et al., 2015). Thus it was inferred that Al-rich gels were formed before the formation of a Si-rich gel (Provis et al., 2015). Fig. 5a additionally indicated that there was a difference in the peak shift patterns for samples with various soluble silicate content (*i.e.* silicate/NaOH ratio). For a sample with sodium silicate/NaOH ratio of one (*i.e.* GPS1), the main peak shift happened after approximately two weeks while for GPS2 and GPS3 (with sodium silicate/NaOH ratio of 2 and 4, respectively) the peak shift occurred earlier. When the Si amount was limited in the reaction environment (which was the case in GPS1 sample with lowest silicate/NaOH ratio) Al dissolution proceeded relatively slowly and even after one week, the Al concentration was not sufficient for the formation of Al-rich gel. However, sufficient Al
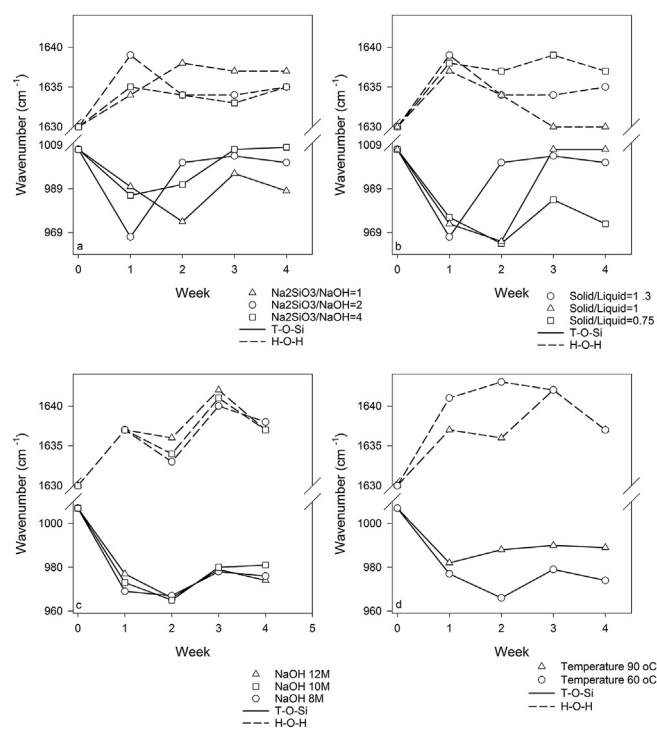

Fig. 5. Comparison of T-O-Si and H-O-H peak positions for different geopolymer samples, (a) samples with different Sodium silicate/NaOH ratio, (b) solid/liquid Ratio, (c) NaOH concentration and (d) Temperature.

was released after two weeks to generate the Al-rich gel phase which eventually resulted in the formation of the Si-rich gel. This result was in agreement with the XRD data for the same sample.

By doubling the sodium silicate ratio (GPS2), the peak for T-O-Si moved to lower wavenumbers after one week which suggested more rapid Al release from the zeolite particles and faster formation of Al-rich gel compared to GPS1. This peak then shifted slightly to higher wavenumbers during the second week which showed the formation of a Si-rich gel. In addition to acceleration in Si and Al species dissolution, the presence of extra silicate in the reaction environment was in favour of the formation of a Si-rich gel. Similar to sample GPS2, in GPS3 with the highest silicate content (sodium silicate/NaOH ratio of 4) the shift to lower wavenumbers happened after one week, but the shift range to the lower wavenumber was shorter than GPS2. As mentioned before, the extra silicates speed up Si-rich gel formation from early reaction stages (less than one week), and for sample GPS3 it possibly happened even faster in comparison with GPS2. These results were again in agreement with the XRD results that showed higher amorphous phase content due to the faster and greater dissolution of zeolite particles in the sample with sodium silicate/NaOH ratios of 2 and 4; in comparison with a sample prepared at a ratio of 1. These results were also in agreement with the outcome of investigations on the effect of sodium silicate/NaOH ratio on the geopolymerization of fly ash (Criado et al., 2007).

Fig. 5 also presented the water peak shifts during the geopolymerization. In general , the shift of the water band changed from *ca.* 1630 to 1640 cm^{-1} as the reaction time increased. The 1630 cm^{-1} band represents water strongly interacting with the initial aluminosilicate, possibly in the cavities. However, as the zeolite dissolved in the NaOH solution the additional water added to the system shifted to *ca.* 1636 cm^{-1} which was indicative of bulk water (Madejova, 2003). This shift also could be due to a deformation vibration of physically adsorbed water molecules inside the

cavities of the aluminosilicate crystalline structure (Pelmenschikov et al., 1995). Notably, the changes of the water molecules peak position seemed to have a relationship with shifts in the peak position of the major bond of T-O-Si ($1007 \, cm^{-1}$) which suggested that the presence of water in the pores influenced the T-O-T vibrations (Sarkany, 1999).

3.3. Influence of the solid to liquid ratio on geopolymerization

Solid/Liquid ratio (S/L) is one of the most significant factors governing the geopolymerization reaction (Khale and Chaudhary, 2007). S/L ratio is known to affect the drying shrinkage during geopolymerization of aluminosilicates (Panias et al., 2007). Therefore, the effect of S/L ratio was investigated at a fixed sodium silicate/NaOH ratio of 2 and sodium hydroxide concentration of 10 M. Three samples with different zeolite/liquid mass ratio of 1.3 (GPS2), 1 (GPS8), and 0.75 (GPS4) were synthesized using the finest zeolite particle size of 54 μm and cured at 60 °C for 1–4 weeks [Table 1].

It can be seen in Fig. 4b that by decreasing the S/L ratio from 1.3 (GPS2) to 0.75 (GPS4), the amorphous phase percentage initially rose by 5% followed by a slight reduction in value in the second week. Although the general trend was similar to that of sample GPS2, the decline after the second week (likely to be due to the reformation of crystals) was smaller and the amorphous content did not change significantly after the second week. The reason for such high amorphous level for GPS4 was that the initial dissolution of Si and Al was strongly dependent upon NaOH quantity. On the other hand, as mentioned earlier, the higher level of sodium silicate present was also able to accelerate the dissolution of Al from aluminosilicate particles and break down the crystalline structure. Therefore, geopolymerization at high NaOH and sodium silicate content when solid content was low, would result in a high amorphous level.

Chemical analysis of the samples using the FTIR technique confirmed the results of XRD analysis. As it is clear in Fig. 5b, decreasing the S/L ratio from 1.3 (GPS2) to 0.75 (GPS4) accelerated the changes resulting in peak shifts for both water (H-O-H) and T-O-Si peaks. It appeared that the higher amount of liquid, and reagents, promoted the rapid formation of a Si-rich gel. The samples with higher liquid content seemed to have lower Al dissolution rate during the second week. This observation suggested that as previously reported (Hajimohammadi and van Deventer, 2016), the formation of Si-rich gel could have reached an equilibrium with Al-rich gel, and subsequently, during the third week, the Si-rich gel formation overcame the Al gel generation.

Increasing solid content from 1 to 1.3 did not have a significant effect on the level of amorphous content. Although the amorphous content was higher at week one, which was unexpected, the amorphous content of GPS2 and GPS8 was similar after two weeks. In spite of the higher conversion of aluminosilicate to geopolymer, samples with relatively high liquid content (GPS4) suffered from efflorescence. This phenomenon happens when extra NaOH in the geopolymer matrix remains unreacted in the geopolymer in the presence of high Na_2O/Al_2O_3 ratios (Najafi Kani et al., 2012). When the liquid content is high, water moving outward through the channels would bring sodium ions to the material surface. As water evaporates, the sodium cations left on the surface react with carbon dioxide (CO_2) from the atmosphere and form a white carbonate layer on the surface.

It's worth mentioning that efflorescence and carbonation of the geopolymers are different phenomena that happen in geopolymerization. Efflorescence is only on the surface and may not have a negative effect on the mechanical properties of the geopolymer. While in carbonation CO_2 and Na^+ existing inside the geopolymer framework react and carbonate deposits from inside the geopolymers. Carbonation generally results in a pH decline and eventually to collapse of the geopolymer structure (Najafi Kani et al., 2012). Unlike carbonation, efflorescence can be easily detected by a visual check. If the higher cost of potassium hydroxide can be justified, this can also be easily controlled by replacing NaOH with KOH since potassium connections to the aluminosilicate gel network are stronger; and also the crystals of potassium carbonate are not usually visibly noticeable compared to the sodium carbonate crystals (Najafi Kani et al., 2012).

3.4. The effect of NaOH concentration upon geopolymer formation

The concentration of the alkali solution is also a critical factor in alkali-activated binders. To evaluate the effect of NaOH concentration on geopolymer properties, three different samples with a concentration of 8 (GPS7), 10 (GPS8) and 12 (GPS6) mole/L were synthesized using zeolite with particle size of 54 μm then cured at 60 °C from 7 to 28 days. It can be seen in Fig. 4c that by increasing NaOH concentration from 8 (GPS7) to 10 M (GPS8) and the maximum amount of 12M (GPS6), the amorphous content increased. It was inferred that higher concentrations of sodium hydroxide caused the zeolite particles to dissolve more readily and thus make amorphous content (Somna et al., 2011). For GPS6, with the highest NaOH concentration of 12M, the amorphous content reached 60% after only one week and remained almost constant afterwards. This situation can be an indication of a high rate of conversion from crystalline aluminosilicate to geopolymer. As evident in Fig. 5c, increasing NaOH concentration from 8 (GPS7) to 12 (GPS6), slightly shortened the range of wavenumber shift of the T-O-Si peak in the FTIR spectra. These results suggested that higher NaOH concentration favoured the Al dissolution rate, formation of Al-rich gel and subsequently Si-rich gel at an early stage of geopolymerization.

It has been reported that aluminosilicate solubility, compressive strength, and flexural strength usually increase with increasing the alkali solution concentration (Liew et al., 2016b). However, in the present study although the amorphous content of samples was greater when the sodium hydroxide concentration increased; the same trend was not replicated for the mechanical strength. For instance, the samples prepared using 12 M NaOH were fragile and their compressive strength was not measurable. One reason for the brittle fracture behaviour of the sample prepared at very high NaOH concentration was the low water content which may have led to incomplete wetting of zeolite particles which inhibited workability. Another explanation was that increasing NaOH concentration above a certain level accelerated dissolution and formation of the amorphous component; but slowed the polycondensation reaction which resulted in a low strength (Phair and Van Deventer, 2002). In other words, at the high sodium hydroxide concentrations, more oligomers were formed due to higher alkalinity; but the oligomers did not grow to polymers.

3.5. The importance of temperature upon geopolymer formation

Temperature plays a vital role in any chemical reaction, and the geopolymerization reaction was not an exception. Therefore, to investigate the effect of this factor on the properties of geopolymer material, two samples GPS6 and GPS7 were synthesized at temperatures of 90 and 60 °C, respectively; using zeolite with a particle size of 54 μm and then cured for 1–4 weeks. XRD analysis indicated the formation of analcime crystals at higher temperature [Fig. 6]. This observation was in agreement with previous reports that indicated that heating of geopolymers at temperatures higher than 85 °C resulted in crystallisation of various minerals (Rovnaník, 2010).
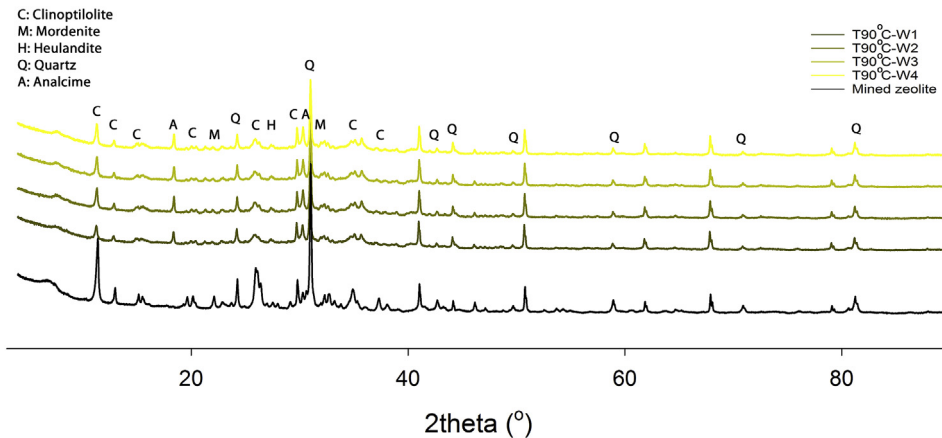
Fig. 6. Formation of analcime in a sample cured at 90 °C.

However, despite the fact that analcime crystals formed, by increasing temperature from 60 to 90 °C the overall crystalline content of the geopolymer declined and the amorphous phase percentage rose by 10% [Fig. 4d]. The reason for the higher amorphous content at elevated temperature was possibly due to the greater extent of the dissolution of Al and Si from zeolite crystals that speeded up the nuclei formation and consequently the polycondensation reaction (Sindhunata et al., 2006). This effect has also been reported in polymerization of other aluminosilicates regardless of the type of alkali hydroxide or SiO_2/M_2O ratios (Sindhunata et al., 2006).

Samples cured at 90 °C in this study exhibited major cracks on the surface and were fragile for mechanical strength tests. Similar outcomes have been reported for other aluminosilicates (Sindhunata et al., 2006; van Jaarsveld et al., 2003) where curing temperatures close to the boiling temperature of water decreased the strength of geopolymers. This was due to the rapid evaporation of water from geopolymer samples which resulted in the microcrack formation in the structure (Bakria et al., 2011; Sindhunata et al., 2006). FTIR spectra of the samples confirmed the results from XRD characterization. As Fig. 5d shows, at the higher temperature of 90 °C (GPS5) the extent of the main peaks' shift (i.e. T-O-Si and H-O-H) was shorter than the sample with curing temperature of 60 °C (suggesting the faster formation of Al-gel at a higher temperature). Table 4 summarizes the main effects observed by changing each parameter.

3.6. Microstructure of geopolymers

Fig. 7 and Fig. 8 compares the SEM images of the mined zeolite and a typical geopolymer sample. The geopolymer sample was taken from GPS4 that was prepared using 10 M NaOH, sodium silicate/sodium hydroxide ratio of 2 and the solid to liquid ratio of 0.75. Curing at 60 °C for four weeks was shown to result in a high amorphous content of 70%. Mined zeolite had an irregular structure
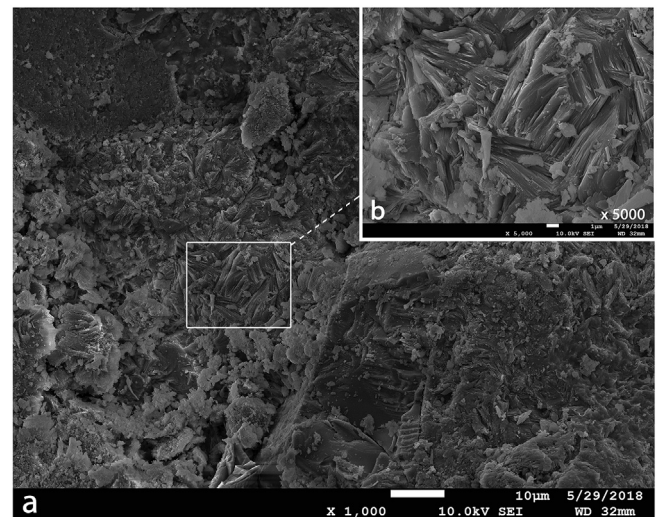

Fig. 7. SEM micrograph of the (a) zeolite morphology with magnification x1,000 (b) magnification x5,000.

which was consistent with the known heterogeneity of mined zeolite materials [Fig. 7a and b]. In contrast the geopolymer sample [Fig. 8] was comprised of random plate features with a suggestion of increased porosity in the structure.

The microstructure of the samples was also characterized at different stages of curing [Fig. 9]. As can be seen in Fig. 9a, the clinoptilolite crystals contained defects caused by the dissolution step in accord with previous reports (Shi et al., 2003). Fig. 9b also shows a crystalline structure which was surrounded by geopolymer. This image was an evidence that some materials are more challenging to dissolve. In this case, the pyramid-shape crystal was indicative of quartz [Fig. 9b] which was identified using EDS

Table 4
Summarized main outcomes of the different effect.

Studied Parameters	Summarized outcome
Particle size of raw mineral	The optimized particle size was found to be 45 μm.
Sodium silicate ratio/NaOH	The best sodium silicate/NaOH mass ratio was 2.
Solid/Liquid ratio	Highest liquid content resulted in a higher amorphous content.
NaOH concentration	The optimized NaOH was determined to be 10M.
Time	The chemical stability achieved after 2 weeks for almost all samples.
Temperature	The geopolymer synthesized at 90 °C resulted in a high amorphous value of 70%.

Fig. 8. Geopolymer sample (GPS4) image with different magnifications after 4 weeks of curing.

Fig. 9. (a) Sample GPS1 after 1 week; (b) quartz crystal; (c) growth of analcime in sample GPS4; (d) chabazite crystals in sample GPS1.

confirming the presence of only silicon and oxygen. SEM also detected the formation of new crystalline phases such as analcime [Fig. 9c]. Analcime content increased to almost 5.5% after 2 weeks of curing at 60 °C and remained intact afterwards. Yarn ball-shaped crystals of chabazite (Zhou et al., 2013) can be seen in the SEM micrograph shown in Fig. 9d. The highest amount of chabazite was detected in samples prepared at a sodium silicate/sodium hydroxide ratio of one (*i.e.* sample GPS1). Data extracted from XRD characterization showed that chabazite content increased to almost 8% after 4 weeks of curing at 90 °C. The zeolitic structure of chabazite contains a broad range of compositions and EDS suggested

that the Si/Al ratio was 2.45 which was in agreement with previous reports on chabazite synthesis (Zhou et al., 2013).

3.7. Thermal stability of geopolymer

Fig. 10 compares not only mass changes but also the thermal behaviour of the mined zeolite and geopolymer. For this test, the temperature was increased from ambient temperature to 100 °C at a rate of 10 °C/min and was kept constant at 100 °C for 20 min to ensure free water was evaporated. Subsequently, heating was continued at the same rate of 10 °C/min up to 1200 °C. As can be
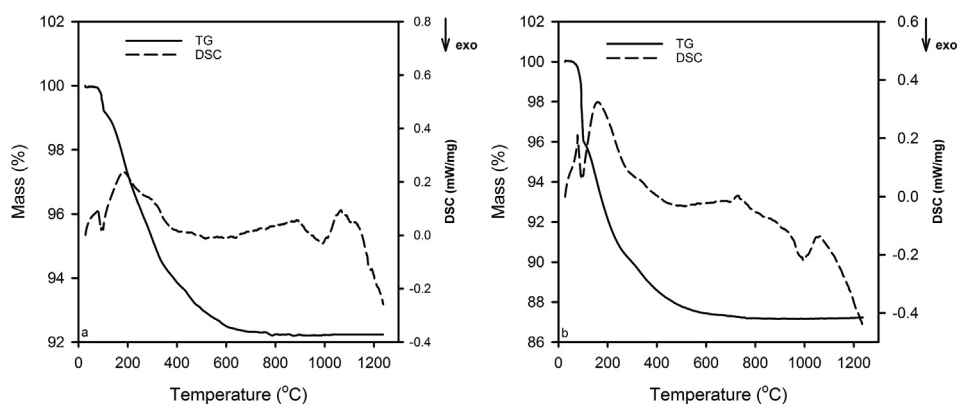
Fig. 10. TG and DSC with a heating rate of 10°C/min (a) mined zeolite (b) geopolymer sample.

seen in the resultant TG curve of zeolite [Fig. 10a] a total mass loss of 7.76 wt% occurred over the temperature range of 25–1200 °C which was ascribed solely to water desorption (Alshameri et al., 2014). Based on the literature, there are three main water types in a zeolite framework: (i) external water, (ii) loosely bound water and (iii) tightly bound water (Knowlton et al., 1981). The external water and loosely bound water are referred to as structural water, water located in the zeolite cavities, and water that is loosely bound to the non-framework cations (Lemougna et al., 2011). In this study, 66% of the weight loss due to water desorption happened at *ca.* 100 °C which was accompanied by lesser water losses at approximately 300 °C (loosely bound water) and below 700 °C (tightly bound water or metal-bound water (Castaldi et al., 2005)). No further reduction in mass was observed after 700 °C but an exothermic peak was observed at approximately 900 °C that was due to the breakdown of zeolite crystallinity.

Thermal characterization of geopolymers showed that the polymerization process did not have a negative effect on the thermal stability of the samples [Fig. 10b]. However, geopolymer had higher water sorption capacity (13% compared to 8% for mined zeolite). Although the amount of external water evaporated at around 100 °C, was not affected by geopolymerization, the weight loss around ~300 °C and ~700 °C was significantly higher for the geopolymer. This observation may be due to greater porosity of geopolymer compared to zeolite (as suggested in the SEM images) (Ulloa et al., 2018). One caveat was that the degradation of chemicals formed during geopolymerization could also contribute to the weight loss in the temperature range 300–700 °C. For instance, decomposition of sodium carbonate at 400 °C (Ulloa et al., 2018) can contribute to this mass loss. At 750 °C, the thermal analysis presented a small endothermic peak that can be ascribed to the viscous sintering process of geopolymer (Zhang et al., 2016).

The source precursors for geopolymer fabrication is usually inorganic natural resources (mined zeolite in this study) that results in a production of more environmentally friendly products. Mined zeolites have great potential for various applications due to their unique exceptional properties such as ion-exchange capacity, and being porous. This study showed the feasibility of geopolymerization of mined zeolite and characterized the sustainable 3D structure of the synthesized geopolymer using different characterization methods. Although there are some studies on geopolymerization of mined zeolite, the microstructure and microchemistry of such materials have not been investigated in depth. For example in a study conducted on geopolymerization of Greek clinoptilolite (Ortega et al., 2000), the crystalline phase only studied qualitatively and the quantitative analyses were underestimated. The quantitative analyses in geopolymerization of

natural resources, give enlightening information about the most reacted phases (crystals), identify the impurities (such as quartz in this study), determine the percentage of formed zeolitic crystals and monitor their growth as a major potential competitor of the amorphous geopolymer structure during geopolymerization and finally determines the amorphous value of the geopolymer. Another example is a study on the alkali activation of Mexican zeolite (Villa et al., 2010) in which the micrographs of the products were provided, but the microstructure of the formed gel (such as the formation of zeolite crystals in the present study) was not well discussed. Geopolymers are difficult to characterize (Antunes Boca Santa et al., 2013) and using crystalline zeolite as the main precursor makes it more challenging, so discussion any observation could help to determine the reaction mechanism and to predict the behaviour of the product and their potential applications. Using of mined zeolite geopolymer as a sustainable construction material and contaminants adsorbent material in water treatment systems are two subjects of future research.

4. Conclusions

Geopolymers were successfully synthesized using mined zeolite. The results indicated that:

a) The finer the zeolite particle size the higher amorphous content in the geopolymer and the higher mechanical strength attained.

b) The higher amorphous content did not necessarily translate to the higher mechanical strength. the formation of oligomers that would not grow to polymers and formation of new crystalline materials were found to be a part of the reason for low mechanical strength.

c) By increasing temperature from 60 °C to 90 °C the overall crystalline content of the geopolymer declined and the amorphous phase percentage rose by 10%.

d) Amorphous content of all samples remained almost constant after 2 weeks at a fixed temperature, suggesting the optimized curing time for a chemically stable zeolite geopolymer.

e) It was proven, using XRD and SEM-EDS that analcime and chabazite crystals formed during geopolymerization.

f) Thermal analysis by TG-DSC confirmed thermal stability to that of raw zeolite.

Technology (QUT) for access to analytical instrumentation, supported by the Faculty of Science and Engineering at QUT. S. Amari acknowledges the support of QUT for her International Postgraduate Research Scholarship.

Appendix A. Supplementary data

Supplementary data to this article can be found online at https://doi.org/10.1016/j.jclepro.2019.06.237.

References

ASTM C39/C39M-03, 2003. Standard Test Method for Compressive Strength of Cylindrical Concrete Specimens. ASTM International, West Conshohocken, PA. www.astm.org.

Aguirre Guerrero, A.M., Robayo-Salazar, R.A., de Gutierrez, R.M., 2017. A novel geopolymer application: coatings to protect reinforced concrete against corrosion. Appl. Clay Sci. 135 (Suppl. C), 437–446. https://doi.org/10.1016/j.clay.2016.10.029.

Alshameri, A., Yan, C.J., Al-Ani, Y., Dawood, A.S., Ibrahim, A., Zhou, C.Y., Wang, H.Q., 2014. An investigation into the adsorption removal of ammonium by salt activated Chinese (Hulaodu) natural zeolite: kinetics, isotherms, and thermodynamics. J. Taiwan Inst. Chem. Eng. 45 (2), 554–564. https://doi.org/10.1016/j.jtice.2013.05.008.

Antunes Boca Santa, R.A., Bernardin, A.M., Riella, H.G., Kuhnen, N.C., 2013. Geopolymer synthetized from bottom coal ash and calcined paper sludge. J. Clean. Prod. 57, 302–307. https://doi.org/10.1016/j.jclepro.2013.05.017.

Bakria, A.M.M.A., Kamarudin, H., BinHussain, M., Nizar, I.K., Zarina, Y., Rafiza, A.R., 2011. The effect of curing temperature on physical and chemical properties of geopolymers. Physics Procedia 22, 286–291. https://doi.org/10.1016/j.phpro.2011.11.045.

Bondar, D., Lynsdale, C., Ramezanianpour, A., Milestone, N., 2007. Alkali Activation of Natural Pozzolan for Geopolymer Cement Production. Int. Conf. Sustain. Construct. Mater. Technol. 313–317.

Castaldi, P., Santona, L., Cozza, C., Giuliano, V., Abbruzzese, C., Nastro, V., Melis, P., 2005. Thermal and spectroscopic studies of zeolites exchanged with metal cations. J. Mol. Struct. 734 (1–3), 99–105. https://doi.org/10.1016/j.molstruc.2004.09.009.

Cheng, T.-W., Chiu, J.P., 2003. Fire-resistant Geopolymer Produce by Granulated Blast Furnace Slag.

Criado, M., Fernandez-Jimenez, A., Palomo, A., 2007. Alkali activation of fly ash: effect of the SiO2/Na2O ratio Part I: FTIR study. Microporous Mesoporous Mater. 106 (1–3), 180–191. https://doi.org/10.1016/j.micromeso.2007.02.055.

Dehghan, R., Anbia, M., 2017. Zeolites for adsorptive desulfurization from fuels: a review. Fuel Process. Technol. 167, 99–116. In: https://doi.org/10.1016/j.fuproc.2017.06.015.

El-Eswed, B.I., Yousef, R.I., Alshaaer, M., Hamadneh, I., Al-Gharabli, S.I., Khalili, F., 2015. Stabilization/solidification of heavy metals in kaolin/zeolite based geopolymers. Int. J. Miner. Process. 137 (Suppl. C), 34–42. https://doi.org/10.1016/j.minpro.2015.03.002.

Elaiopoulos, K., Perraki, T., Grigoropoulou, E., 2010. Monitoring the effect of hydrothermal treatments on the structure of a natural zeolite through a combined XRD, FTIR, XRF, SEM and N2-porosimetry analysis. Microporous Mesoporous Mater. 134 (1–3), 29–43. https://doi.org/10.1016/j.micromeso.2010.05.004.

Fernandez-Jimenez, A., Palomo, A., Criado, M., 2005. Microstructure development of alkali-activated fly ash cement: a descriptive model. Cement Concr. Res. 35 (6), 1204–1209. https://doi.org/10.1016/j.cemconres.2004.08.021.

Ferone, C., Capasso, I., Bonati, A., Roviello, G., Montagnaro, F., Santoro, L., Turco, R., Cioffi, R., 2019. Sustainable management of water potabilization sludge by means of geopolymers production. J. Clean. Prod. 229, 1–9. https://doi.org/10.1016/j.jclepro.2019.04.299.

Ghafoori, N., Najimi, M., Radke, B., 2016. Natural Pozzolan-based geopolymers for sustainable construction. Environ. Earth Sci. 75 (14), 1110. https://doi.org/10.1007/s12665-016-5898-5.

Hajimohammadi, A., Provis, J.L., van Deventer, J.S.J., 2011. The effect of silica availability on the mechanism of geopolymerisation. Cement Concr. Res. 41 (3), 210–216. https://doi.org/10.1016/j.cemconres.2011.02.001.

Hajimohammadi, A., van Deventer, J.S.J., 2016. Dissolution behaviour of source materials for synthesis of geopolymer binders: a kinetic approach. Int. J. Miner. Process. 153 (Suppl. C), 80–86. https://doi.org/10.1016/j.minpro.2016.05.014.

Khale, D., Chaudhary, R., 2007. Mechanism of geopolymerization and factors influencing its development: a review. J. Mater. Sci. 42 (3), 729–746. https://doi.org/10.1007/s10853-006-0401-4.

Knowlton, G.D., White, T.R., Mckague, H.L., 1981. Thermal study of types of water associated with clinoptilolite. Clay Clay Miner. 29 (5), 403–411. https://doi.org/10.1346/Ccmn.1981.0290510.

Komljenovic, M., Bascarevic, Z., Bradic, V., 2010. Mechanical and microstructural properties of alkali-activated fly ash geopolymers. J. Hazard Mater. 181 (1–3), 35–42. https://doi.org/10.1016/j.jhazmat.2010.04.064.

Lemougna, P.N., MacKenzie, K.J.D., Melo, U.F.C., 2011. Synthesis and thermal properties of inorganic polymers (geopolymers) for structural and refractory applications from volcanic ash. Ceram. Int. 37 (8), 3011–3018. https://doi.org/10.1016/j.ceramint.2011.05.002.

Liew, Y.-M., Heah, C.-Y., Mohd Mustafa, A.B., Kamarudin, H., 2016a. Structure and properties of clay-based geopolymer cements: a review. Prog. Mater. Sci. 83 (Suppl. C), 595–629. https://doi.org/10.1016/j.pmatsci.2016.08.002.

Liew, Y.-M., Heah, C.-Y., Mohd Mustafa, A.B., Kamarudin, H., 2016b. Structure and properties of clay-based geopolymer cements: a review. Prog. Mater. Sci. 83, 595–629. https://doi.org/10.1016/j.pmatsci.2016.08.002.

Liew, Y.M., Kamarudin, H., Al Bakri, A.M.M., Bnhussain, M., Luqman, M., Nizar, I.K., Ruzaidi, C.M., Heah, C.Y., 2012. Optimization of solids-to-liquid and alkali activator ratios of calcined kaolin geopolymeric powder. Constr. Build. Mater. 37, 440–451. https://doi.org/10.1016/j.conbuildmat.2012.07.075.

Madejova, J., 2003. FTIR techniques in clay mineral studies. Vib. Spectrosc. 31 (1), 1–10. https://doi.org/10.1016/S0924-2031(02)00065-6.

Majidi, B., 2009. Geopolymer technology, from fundamentals to advanced applications: a review. Mater. Technol. 24 (2), 79–87. https://doi.org/10.1179/175355509x449355.

Mehta, A., Siddique, R., 2016. An overview of geopolymers derived from industrial by-products. Constr. Build. Mater. 127, 183–198. https://doi.org/10.1016/j.conbuildmat.2016.09.136.

Millar, G.J., Couperthwaite, S.J., Alyuz, K., 2016. Behaviour of natural zeolites used for the treatment of simulated and actual coal seam gas water. J. Environ. Chem. Eng. 4 (2), 1918–1928. https://doi.org/10.1016/j.jece.2016.03.014.

Ming, L.Y., 2011. Investigating the possibility of utilization of kaolin and the potential of metakaolin to produce green cement for construction purposes-A review. Aust. J. Basic Appl. Sci. 5 (9), 9.

Mumpton, F.A., 1960. Clinoptilolite redefined. Am. Mineral. 45 (3–4), 351–369.

Najafi Kani, E., Allahverdi, A., Provis, J.L., 2012. Efflorescence control in geopolymer binders based on natural pozzolan. Cement Concr. Compos. 34 (1), 25–33. https://doi.org/10.1016/j.cemconcomp.2011.07.007.

Najimi, M., 2016. Alkali-Activated Natural Pozzolan/Slag Binder for Sustainable Concrete.

Nikolov, A., Rostovsky, I., Nugteren, H., 2017. Geopolymer materials based on natural zeolite. Case Stud. Constr. Mater. 6 (Suppl. C), 198–205. https://doi.org/10.1016/j.cscm.2017.03.001.

Nyale, S.M., Eze, C.P., Akinyeye, R.O., Gitari, W.M., Akinyemi, S.A., Fatoba, O.O., Petrik, L.F., 2014. The leaching behaviour and geochemical fractionation of trace elements in hydraulically disposed weathered coal fly ash. J Environ Sci Health A Tox Hazard Subst Environ Eng 49 (2), 233–242. https://doi.org/10.1080/10934529.2013.838929.

Ortega, E.A., Cheeseman, C., Knight, J., Loizidou, M., 2000. Properties of alkali-activated clinoptilolite. Cement Concr. Res. 30 (10), 1641–1646. https://doi.org/10.1016/S0008-8846(00)00331-8.

Panda, B., Paul, S.C., Hui, L.J., Tay, Y.W.D., Tan, M.J., 2017. Additive manufacturing of geopolymer for sustainable built environment. J. Clean. Prod. 167, 281–288. https://doi.org/10.1016/j.jclepro.2017.08.165.

Panias, D., Giannopoulou, I.P., Perraki, T., 2007. Effect of synthesis parameters on the mechanical properties of fly ash-based geopolymers. Colloid. Surf. Physicochem. Eng. Asp. 301 (1–3), 246–254. https://doi.org/10.1016/j.colsurfa.2006.12.064.

Papa, E., Medri, V., Amari, S., Manaud, J., Benito, P., Vaccari, A., Landi, E., 2018. Zeolite-geopolymer composite materials: production and characterization. J. Clean. Prod. 171 (Suppl. C), 76–84. https://doi.org/10.1016/j.jclepro.2017.09.270.

Pelmenschikov, A.G., Vanwolput, J.H.M.C., Janchen, J., Vansanten, R.A., 1995. (a,B,C) triplet of infrared oh bands of zeolitic H-complexes. J. Phys. Chem. 99 (11), 3612–3617. https://doi.org/10.1021/j100011a031.

Phair, J.W., Van Deventer, J.S.J., 2002. Effect of the silicate activator pH on the microstructural characteristics of waste-based geopolymers. Int. J. Miner. Process. 66 (1–4), 121–143. https://doi.org/10.1016/S0301-7516(02)00013-3.

Pimraksa, K., Chindaprasirt, P., Rungchet, A., Sagoe-Crentsil, K., Sato, T., 2011. Lightweight geopolymer made of highly porous siliceous materials with various Na2O/Al2O3 and SiO2/Al2O3 ratios. Mater. Sci. Eng. A 528 (21), 6616–6623. https://doi.org/10.1016/j.msea.2011.04.044.

Provis, J.L., Bernal, S.A., 2014. Geopolymers and related alkali-activated materials. Annu. Rev. Mater. Res. 44 (1), 299–327, 44. https://doi.org/10.1146/annurev-matsci-070813-113515.

Provis, J.L., Palomo, A., Shi, C.J., 2015. Advances in understanding alkali-activated materials. Cement Concr. Res. 78, 110–125. https://doi.org/10.1016/j.cemconres.2015.04.013.

Rahier, H., Denayer, J.F., Van Mele, B., 2003. Low-temperature synthesized aluminosilicate glasses - Part IV - modulated DSC study on the effect of particle size of metakaolinite on the production of inorganic polymer glasses. J. Mater. Sci. 38 (14), 3131–3136. https://doi.org/10.1023/A:1024733431657.

Rao, F., Liu, Q., 2015. Geopolymerization and its potential application in mine tailings consolidation: a review. Miner. Process. Extr. Metall. Rev. 36 (6), 399–409. https://doi.org/10.1080/08827508.2015.1055625.

Reddy, M.S., Dinakar, P., Rao, B.H., 2016. A review of the influence of source material's oxide composition on the compressive strength of geopolymer concrete. Microporous Mesoporous Mater. 234 (Suppl. C), 12–23. https://doi.org/10.1016/j.micromeso.2016.07.005.

Rovnaník, P., 2010. Effect of curing temperature on the development of hard structure of metakaolin-based geopolymer. Constr. Build. Mater. 24 (7), 1176–1183. https://doi.org/10.1016/j.conbuildmat.2009.12.023.

Sarkany, J., 1999. Effects of water and ion-exchanged counterion on the FTIR spectra

of ZSM-5. I. NaH-ZSM-5: H-bonding with OH groups of zeolite and formation of H+(H2O)(n). Appl. Catal. Gen. 188 (1—2), 369—379. https://doi.org/10.1016/S0926-860x(99)00257-4.

Shi, C., Roy, D., Krivenko, P., 2003. Alkali-Activated Cements and Concretes. Chapman and Hall/CRC, London, UNITED KINGDOM.

Sindhunata, van Deventer, J.S.J., Lukey, G.C., Xu, H., 2006. Effect of curing temperature and silicate concentration on fly-ash-based geopolymerization. Ind. Eng. Chem. Res. 45 (10), 3559—3568. https://doi.org/10.1021/ie051251p.

Somna, K., Jaturapitakkul, C., Kajitvichyanukul, P., Chindaprasirt, P., 2011. NaOH-activated ground fly ash geopolymer cured at ambient temperature. Fuel 90 (6), 2118—2124. https://doi.org/10.1016/j.fuel.2011.01.018.

Temuujin, J., van Riessen, A., 2009. Effect of fly ash preliminary calcination on the properties of geopolymer. J. Hazard Mater. 164 (2—3), 634—639. https://doi.org/10.1016/j.jhazmat.2008.08.065.

Ulloa, N.A., Baykara, H., Cornejo, M.H., Rigail, A., Paredes, C., Villalba, J.L., 2018. Application-oriented mix design optimization and characterization of zeolite-based geopolymer mortars. Constr. Build. Mater. 174, 138—149. https://doi.org/10.1016/j.conbuildmat.2018.04.101.

van Jaarsveld, J.G.S., van Deventer, J.S.J., Lukey, G.C., 2003. The characterisation of source materials in fly ash-based geopolymers. Mater. Lett. 57 (7), 1272—1280.

https://doi.org/10.1016/s0167-577x(02)00971-0.

Villa, C., Pecina, E.T., Torres, R., Gomez, L., 2010. Geopolymer synthesis using alkaline activation of natural zeolite. Constr. Build. Mater. 24 (11), 2084—2090. https://doi.org/10.1016/j.conbuildmat.2010.04.052.

Wang, S., Li, L., Zhu, Z.H., 2007. Solid-state conversion of fly ash to effective adsorbents for Cu removal from wastewater. J. Hazard Mater. 139 (2), 254—259. https://doi.org/10.1016/j.jhazmat.2006.06.018.

Xu, H., Van Deventer, J.S.J., 2000. The geopolymerisation of alumino-silicate minerals. Int. J. Miner. Process. 59 (3), 247—266. https://doi.org/10.1016/S0301-7516(99)00074-5.

Xu, H., van Deventer, J.S.J., 2003. Effect of source materials on geopolymerization. Ind. Eng. Chem. Res. 42 (8), 1698—1706. https://doi.org/10.1021/ie0206958.

Zhang, H.Y., Kodur, V., Wu, B., Cao, L., Wang, F., 2016. Thermal behavior and mechanical properties of geopolymer mortar after exposure to elevated temperatures. Constr. Build. Mater. 109, 17—24. https://doi.org/10.1016/j.conbuildmat.2016.01.043.

Zhou, R., Li, Y., Liu, B., Hu, N., Chen, X., Kita, H., 2013. Preparation of chabazite membranes by secondary growth using zeolite-T-directed chabazite seeds. Microporous Mesoporous Mater. 179, 128—135. https://doi.org/10.1016/j.micromeso.2013.06.003.